



CHALMERS
UNIVERSITY OF TECHNOLOGY

Solubilizing Benzodifuranone-Based Conjugated Copolymers with Single-Oxygen-Containing Branched Side Chains

Downloaded from: <https://research.chalmers.se>, 2025-12-04 20:04 UTC

Citation for the original published paper (version of record):

R. Hinojosa, D., J. Pataki, N., Rossi, P. et al (2024). Solubilizing Benzodifuranone-Based Conjugated Copolymers with Single-Oxygen-Containing Branched Side Chains. *ACS Applied Polymer Materials*, 6(1): 457-465.
<http://dx.doi.org/10.1021/acsapm.3c02137>

N.B. When citing this work, cite the original published paper.

Solubilizing Benzodifuranone-Based Conjugated Copolymers with Single-Oxygen-Containing Branched Side Chains

Diego R. Hinojosa, Nathan J. Pataki, Pietro Rossi, Andreas Erhardt, Shubhradip Guchait, Francesca Pallini, Christopher McNeill, Christian Müller, Mario Caironi,* and Michael Sommer*



Cite This: <https://doi.org/10.1021/acscapm.3c02137>



Read Online

ACCESS |

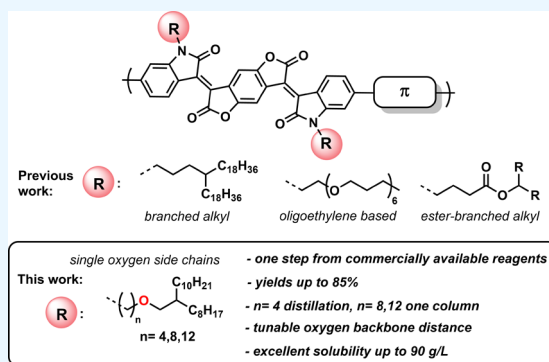
Metrics & More

Article Recommendations

Supporting Information

ABSTRACT: Single-oxygen-containing branched side chains are designed and used to solubilize n-type copolymers consisting of BDF (benzodifuranone), isatin, and thiophene-based units. We present a simple synthetic approach to side chains with varying linker distances between the backbone and the branching point. The synthetic pathway is straightforward and modular and starts with commercially available reagents. The side chains give rise to excellent solubilities of BDF-thiophene copolymers of up to 90 mg/mL, while still being moderate in size (26–34 atoms large). The excellent solubility furthermore allows high molar mass materials. BDF-thiophene copolymers are characterized in terms of optoelectronic and thermoelectric properties. The electrical conductivity of chemically doped polymers is found to scale with molar mass, reaching ~ 1 S/cm for the highest molar mass and longest backbone-branching point distance.

KEYWORDS: solubility, benzodifuranone polymers, n-type conjugated polymers, branched side chains, branching point variation, organic thermoelectrics



1. INTRODUCTION

Since their discovery, conjugated polymers (CPs) have attracted much attention due to their unique properties.^{1,2} In most cases, CPs comprise two main parts: a π -conjugated backbone, responsible for the optoelectronic properties of the final material and side chains. Side chains are flexible, differently, large pendant groups grafted onto the π -backbone of the polymer.³ The tremendous synthetic freedom in the modulation of these groups allows the design of functional side chains that bestow special properties on the macromolecule. For example, introducing ionic groups furnishes conjugated polyelectrolytes that can be processed from water and other polar solvents for application as polymer light-emitting diodes (PLEDs)⁴ and polymer-based photovoltaic cells.⁵ End-chain functionalized side chains, consisting of reactive groups, have also been reported as dormant reactive groups to be further reacted via post-polymerization to achieve different properties.^{6–10} Modification of the electronic properties of the π -conjugated backbone is also possible via side-chain engineering. Directly connecting electron-donating groups^{11–13} or electron-withdrawing groups^{14–17} onto the main chain allows to control the electronic density in the backbone, thus aiding in the modulation of the highest occupied molecular orbital (HOMO) and lowest unoccupied molecular orbital (LUMO) energy levels in the polymer.

Among the most advantageous properties of conjugated polymers is the possibility to process them from solution.

Therefore, the use of side chains to induce solubilization is a key and largely exploited aspect, but side chains are also crucial for the ordering of conjugated polymers in the solid state.^{18,19} The most common side chains used for this purpose are alkyl and oligoethylene glycol (OEG) chains, with the latter allowing better solubility in more polar organic solvents. Both types can be found as linear or branched species. Solubility and the propensity to form ordered domains are only some of the properties affected by the choice of the different side chain types, as shown for instance by diketopyrrolopyrrole copolymers.^{20,21} Branched alkyl side chains increase solubility in general.²² Their use is commonly required in the case of large backbone structures with a high degree of coplanarity.^{23,24} As the backbone twisting decreases, the π - π interactions between chains increase, which reduces solubility and poses limitations to the parameter space for processing from solution. Introducing a branching point also profoundly affects the final polymer structure and performance, with a longer distance between the conjugated backbone and the

Received: September 8, 2023

Revised: November 22, 2023

Accepted: November 27, 2023

branching point reducing sterical hindrance and allowing for better packing, and finally improved performance.^{25–28}

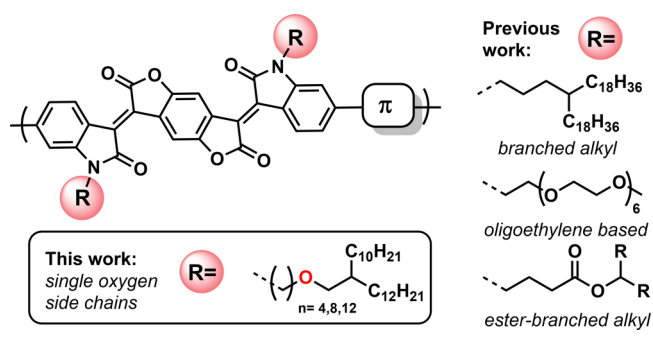
Nonsymmetrical branched side chains are customarily prepared from commercially available Gruebert alcohol precursors.²⁹ Normally, these alcohols need to be transformed to either an electrophilic reagent that is substituted later by a nucleophile in the monomer as done for instance with diketopyrrolopyrroles (DPP),³⁰ or to a nucleophilic amine that reacts with an anhydride for imide-based polymers, as, e.g., naphthalene diimides.³¹ Symmetrically branched side chains on the other hand are tedious to prepare;³² their preparation involves multistep synthetic processes, multiple columns, and purification techniques that reduce the overall polymer yield and increase the total cost.³³ Furthermore, modulation of the branching point in these systems is cumbersome due to their lengthy synthetic pathway.

Benzodifuranone (BDF) is an electron-deficient building block that has most recently been used to prepare self-doping homopolymers with conductivities of up to 6000 S cm⁻¹.^{34,35} However, extension and modification of the BDF core, e.g., by conjugation to isatin units, and finally copolymerization with comonomers, is required to modulate *n*-type properties for multiple application scenarios.^{36–38} Conjugated polymers with BDF cores often show intermolecular hydrogen bonding which enables highly planarized structures and close backbone contacts that result in better charge carrier transport properties.^{39,40} BDF copolymers in which the neighbored isatin units are unsubstituted require less synthetic steps but also exhibit modest electrical conductivities of up to 0.26 S cm⁻¹ upon doping.³⁶ Derivatization of the isatin unit improves electrical conductivities to values of 14 S cm⁻¹, but additional synthetic steps are required that add up to the overall cost of the material. Generally, improved properties of BDF-containing polymers commonly correlate with coplanar backbones, which pose a challenge in terms of solubility. The vast majority of studies carried out with BDF polymers have made use of rather large, branched alkyl side chains consisting of a linear C_x spacer and symmetric, long branches (C₁₈).⁴¹ While providing solubility, the synthesis of such branched alkyl side chains suffers from lengthy synthetic pathways, cumbersome purification, and low overall yields. Moreover, air- and moisture-sensitive Grignard reagents are involved in their preparation, further complicating synthesis and scale-up.³³ In this context it is noteworthy that a variation of the length of the linear spacer is highly beneficial for the optimization of electron mobility for this class of copolymers, and hence synthetic approaches aiming at simplification of synthetic routes are highly desirable.⁴²

For applications involving molecular doping, linear polar side chains of the OEG have been used. However, strong aggregation produces poor miscibility in solution between the polymer and dopant, and phase separation in films, which results in lower electrical conductivity.⁴³ Branched alkyl side chains with ester groups have also been presented.⁴⁴ These offer modularity in terms of the side chain length and ester positioning but are susceptible to hydrolysis, limiting long-term stability and preventing their use in greener polymerization methods such as direct arylation polycondensation (DAP) requiring basic conditions.

The present work introduces single oxygen-containing branched side chains and uses them for solubilizing unsubstituted BDF-containing copolymers (Scheme 1). The side chains can be prepared in one step from commercially

Scheme 1. Overview of Side Chain Systems Used for BDF Copolymers and Scope of This Work



available and economic reagents through a simple Williamson etherification reaction and do not require lengthy purification protocols. The availability of different α , ω -dibromo alkyl spacers, and various Guerbert alcohols render this approach ideal for tuning the backbone-oxygen distance as well as the backbone-branching point distance by choosing different starting materials. Thanks to a chemically robust ether moiety, their synthesis is straightforward and highly modular in terms of spacer and branch length, and the side chains render BDF-based copolymers highly soluble. The presented protocol also enables BDF-isatin monomer synthesis on the gram scale. The ether functionality in the side chain provides high flexibility and leads to excellent solubilities of BDF-isatine-thiophene copolymers up to ~90 mg/mL in *o*-dichlorobenzene (*o*-DCB). Finally, high molar mass copolymers are feasible with conductivities up to 1 S cm⁻¹ upon chemical doping, which outperform similar unsubstituted BDF copolymers reported so far.

2. EXPERIMENTAL SECTION

All details regarding starting materials, methods, synthesis of monomers and polymers, and their characterizations are given in the [Supporting Information](#).

3. RESULTS AND DISCUSSION

3.1. Synthesis and Characterization of BDF Copolymers with Single-Oxygen-Containing Side Chains.

In order to introduce modular, yet simple, side chains that allow for high solubilities, we first *N*-alkylated bromoisatin with 3-bromo-1-propanol furnishing *N*-propan-1-ol-6-bromoisatin, following O-alkylation with 1-iodo-2-octyldodecane (Scheme 2a). While the *N*-alkylation of the isatin proceeded smoothly, the O-alkylation required harsher reaction conditions that led to isatin decomposition. This reduced the yield of the final product and made purification tedious. Furthermore, the necessity of the preparation of the halogenated branched alkyl intermediate also lengthened the overall reaction sequence. A simpler route was then envisaged, in which the side chain was made first, followed by the more straightforward *N*-alkylation of bromoisatin (Scheme 2b). Starting from an excess of commercially available α - ω -dibromoalkanes and Guerbet²⁹ alcohols, the branched halogenated ethers **1a–c** could be obtained under Williamson etherification conditions in good yields. Purification was simplified by using a silica plug and distillation in the case of **1a** and a single column in the case of both **1b** and **1c**.

The simplicity of the synthesis protocol shown in Scheme 2b enabled the use of a range of α - ω -dibromoalkanes with

Scheme 2. (a) Failed Attempts To Synthesize Single Oxygen Side Chains Attached to Isatin Building Blocks; (b) Successful Route to the Synthesis of Single Oxygen Side Chain Containing Bromoisatins **2a–c** and Corresponding Benzodifuranone Monomers **3a–c**; (c) Stille Polycondensation of the Different Monomers **3a–c** to Get Copolymers **P1–P4**

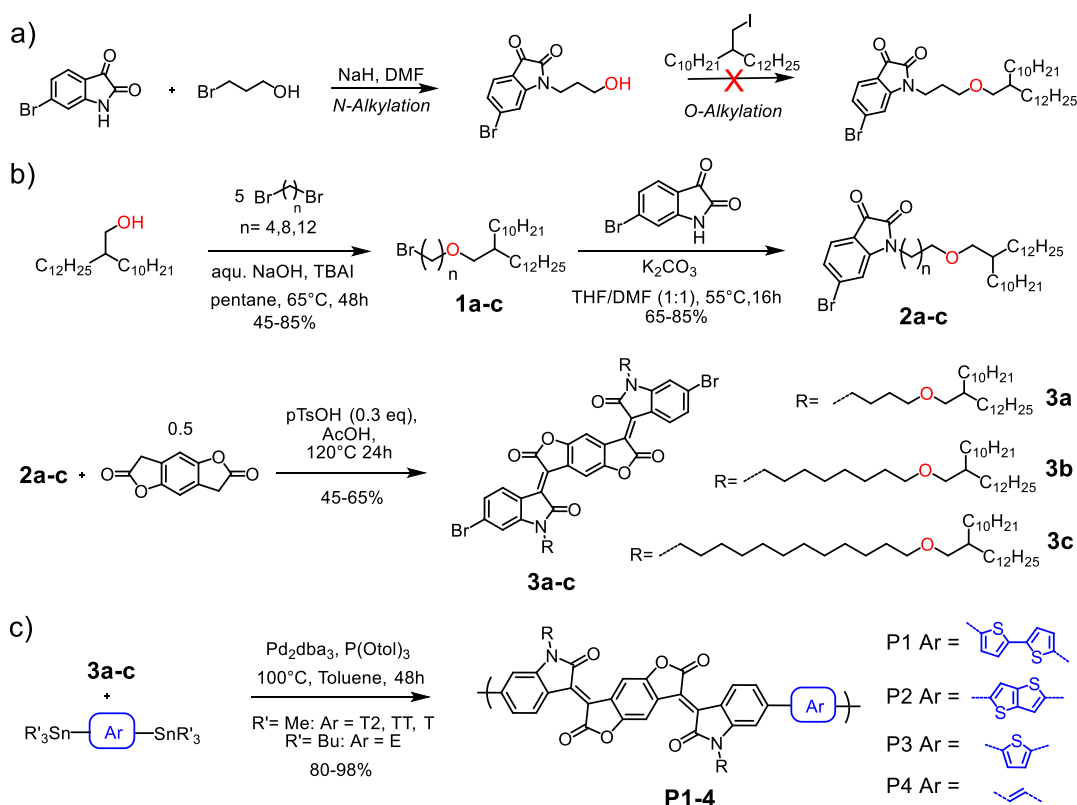


Table 1. Molecular Weights, Dispersities, Yields, and Solubilities of Copolymers **P1–P4**

entry	polymer	side chain/comonomer Ar	M_n [kg/mol]	\bar{D}	yield [%]	solubility [mg/mL]
1	P1a	4O/T2	n.d. ^a	n.d	97	3
2	P2a	4O/TT	n.d. ^a	n.d	98	7
3	P3a	4O/T	50.0	2.0	95	89
4	P3b	8O/T	55.3	1.8	95	70
5	P3c ⁵⁵	12O/T	54.9	2.5	98	92
6	P3c ⁴⁷	12O/T	46.5	1.9	92	n.d.
7	P3c ⁴⁶	12O/T	46.1	1.7	87	n.d.
8	P3c ⁴²	12O/T	42.0	1.5	89	n.d.
9	P3c ²⁸	12O/T	28.0	1.5	85	n.d.
10	P4a	4O/E	10.5	2.6	80	n.d.

^a M_n could not be determined due to low solubility and difficulties in SEC sample preparation. The superscript in entries 5–9 indicates the $M_{n,SEC}$ value of the batch.

varying lengths. Thus, alkylated isatin derivatives **2a–c** were obtained in good yields. Finally, BDF-based monomers **3a–c** were obtained via acidic aldol condensation of the *N*-alkylated isatins and the benzodifuranone core. All intermediates with side chains were thoroughly characterized by nuclear magnetic resonance (NMR) spectroscopy and mass spectrometry (MS) (see Supporting Information Figures S10–S28). Monomer **3a** was used for comonomer screening under Stille polymerization conditions. This cross-coupling variant is the method of choice since the lactone motif of BDF is prone to hydrolysis under basic conditions.⁴⁵ Variation of the stannylated coupling partner furnished polymer series **P1–P4** (Scheme 2c). The polymers were obtained in good to excellent yields and with high number-average molecular weights M_n as measured by size exclusion chromatography (SEC) in 1,2,4-trichloroben-

zene at 150 °C. Only **P4** with stannylated ethylene as a comonomer exhibited low molar mass resulting from reduced reactivity. The properties of all copolymers are summarized in Table 1.

3.2. Side Chain Alkyl Spacer Length Variation and Electronic Performance. Thiophene was used as a reference comonomer, furnishing a series of copolymers **P3a–c** with side chain and molar mass variation as shown in Table 1. For this series, the ether oxygen is located at distances of 4, 8, or 12 carbons from the backbone. Reasonably high M_n values around ~50–55 kg/mol were obtained for all three side chain lengths, indicating that stoichiometry and/or end group degradation may be limiting factors here. The similarity in molecular weights may further result from similar solubilities. We determined the solubility of the polymers quantitatively.⁴⁶

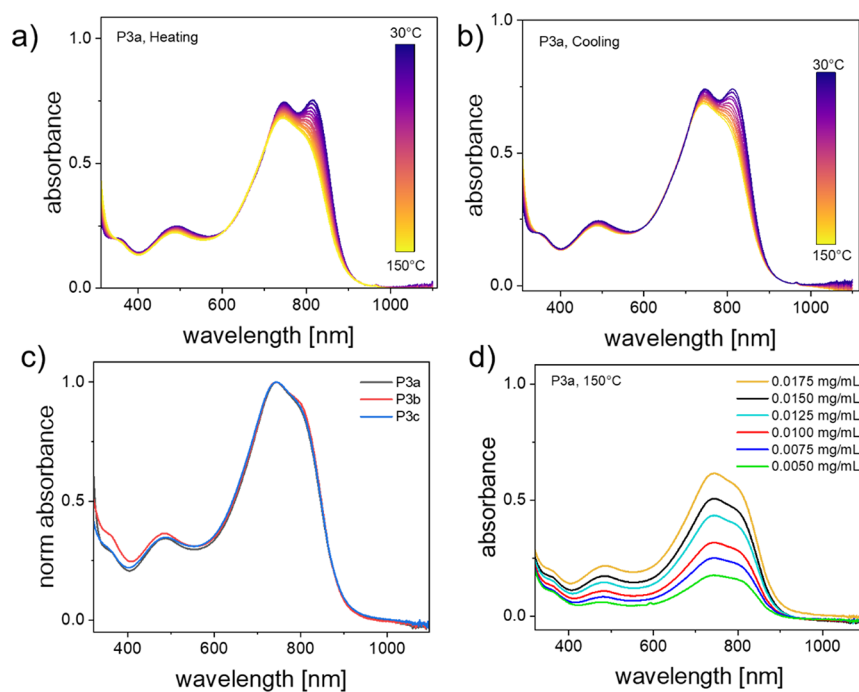


Figure 1. (a) Variable temperature UV–vis spectra of P3a (0.02 mg/mL) in *o*-DCB heating from 30 to 150 °C. (b) Variable temperature UV–vis spectra of P3a (0.02 mg/mL) in *o*-DCB cooling from 150 to 30 °C. (c) UV–vis spectra of 0.02 mg/mL P3a, P3b and P3c at 150 °C in *o*-DCB. (d) UV–vis spectra of P3a at different polymer concentrations in *o*-DCB at 150 °C.

Values of up to 92 mg/mL in *o*-DCB at 150 °C were observed for P3c, representing the highest solubility in the polymer series (Figures 1a, S1).

To better understand solubility-dependent aggregation in solution, a variable temperature UV–vis study of P3a–c in *o*-DCB was conducted (Figures 1b, S2 and S3). From 30 to 150 °C, the shoulder at ~820 nm decreased in intensity as more conformations with larger dihedral angles became accessible.^{46,47} Upon cooling the solution from 150 to 30 °C, the original spectrum was restored, indicating a reversible process. A comparison of the optical absorption spectra of the three different polymers P3a, P3b, and P3c revealed only small differences with respect to varying shoulder intensities for P3b, in good agreement with the lowest solubility of this copolymer.

The optoelectronic properties of the polymers were characterized by cyclic voltammetry (CV) and steady-state absorbance spectroscopy in *o*-DCB solution and in thin film (Table 2). The predominant electron-withdrawing effect of the BDF monomer dominates the electron affinity of the material. Thus, all copolymers exhibited deep LUMO levels around –4.0 eV measured by CV in solution and in film (Figures S4 and S5). The UV–vis spectra of solutions and thin films revealed a blue shift of the vibronic transitions as the donor strength of the comonomer increased, in good agreement with the push–pull character of the system. Strong aggregation in the *o*-DCB solution can be observed for the thiophene-based polymers P1–P3 (Figure S6). Aggregation band intensity decreases from P1 to P3. This is expected, as bithiophene and thienothiophene enable larger π stacking areas and more linear backbone geometries compared to thiophene. Although all polymers P1–4 were found to be soluble in hot *o*-DCB, bithiophene (P1) and thienothiophene (P2) copolymers were less readily dissolved, yielding gelled mixtures that were difficult to process, even at low concentrations. For this reason, P3, with thiophene as the comonomer, was selected as the

Table 2. Summary of the Optoelectronic Properties of P1–P4^a

entry	polymer	$\lambda_{\max, \text{sol}}$ [nm]	band gap _{sol} [eV]	$\lambda_{\max, \text{film}}$ [nm]	band gap _{film} [eV]	HOMO/LUMO _{film} [eV]
1	P1a	860	1.28	843	1.29	–5.47/–4.15
2	P2a	831	1.34	825	1.34	–5.51/–4.02
3	P3a	812	1.35	815	1.34	–5.55/–4.06
4	P3b ⁵⁵	812	1.36	n.d.	n.d.	n.d.
5	P3c ⁵⁵	812	1.34	n.d.	n.d.	n.d.
6	P3c ⁴⁶	n.d.	n.d.	n.d.	n.d.	n.d.
7	P3c ⁴²	n.d.	n.d.	n.d.	n.d.	n.d.
8	P3c ²⁸	n.d.	n.d.	n.d.	n.d.	n.d.
9	P4a	800	1.29	690	1.43	–4.80/–3.51

^aThe superscript of the polymers indicates number average molecular weights from SEC $M_{n, \text{SEC}}$. n.d., not determined.

reference polymer for the study of the electrical and solubility properties.

Well-studied molecular *n*-dopants 4-(1,3-dimethyl-2,3-dihydro-1*H*-benzoimidazol-2-yl)-*N,N*-dimethylaniline (*N*-DMBI) and 4-(1,3-dimethyl-2,3-dihydro-1*H*-benzoimidazol-2-yl)-*N,N*-diphenylaniline (*N*-DPBI) were used to investigate the *n*-doped characteristics of spin-cast polymer films.^{48,49} A first confirmation of the effective doping with *N*-DMBI and *N*-DPBI is obtained from the spin-casted thin film absorption spectrum of P3a coprocessed with *N*-DMBI of varying concentration. Doping levels were determined as molar ratios (MR%) of 40 MR%, 60 MR%, and 80 MR% (Figure 2). The absorbance spectrum of pristine P3a is characterized by prominent features at 740 and 810 nm corresponding to the 0–1 and 0–0 vibronic transitions, respectively, where the 0–1 peak shows slightly stronger absorption. Upon addition of *N*-DMBI (Figure 2) the spectra of P3a are characterized by a sharp bleaching of both 0–1 and 0–0 features, but there is a

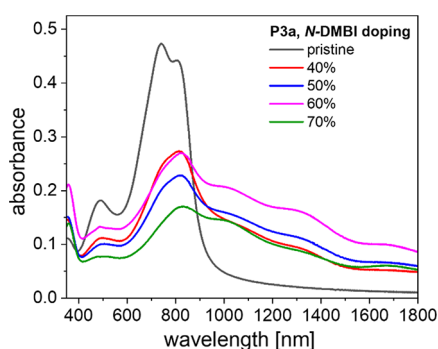


Figure 2. UV-vis-NIR spectra of spin-cast thin films of **P3a** doped with *N*-DMBI.

stronger bleaching of the 0–1 peak compared to that of the 0–0 peak. At 40 MR% *N*-DMBI doping, the 0–0 absorption is stronger than the 0–1 peak, reversing the relationship from the pristine film. As the doping concentration increases to 80 MR% the 0–1 shoulder almost entirely fades with respect to the 0–0 band. A slight redshift in the absorbance of the 0–0 band can also be seen as doping concentration increases. In addition to the bleaching of the vibronic bands in the visible range, the appearance of broad NIR polaron absorption bands centered around 1020, 1320 and 1690 nm, can be seen. As *N*-DMBI doping concentration increases and bleaching of the vibronic bands intensifies, the intensity of these polaronic bands also increase. Additionally, the stability under air of doped films of **P3a** was also investigated (Figure S7).

Upon coprocessing **P3a** with *N*-DPBI, the resulting absorption spectra displayed similarities to the *N*-DMBI doped samples, but the intensity of the vibronic bleaching is reduced and the polaronic NIR bands are of weaker appearance (Figure S8). The differences between the doped samples indicate a higher concentration of charged polymer species in the *N*-DMBI-doped samples, which can be linked to an enhanced carrier density. To reinforce this assertion, the electrical conductivity, σ , of the doped thin films was measured and the *N*-DMBI-doped films were found to have a $\sigma_{\max} = 0.2 \text{ S cm}^{-1}$ while the *N*-DPBI-doped films exhibited a $\sigma_{\max} = 0.1 \text{ S cm}^{-1}$ at 60 MR%.

Due to the superior performance of **P3a** with *N*-DMBI, this dopant was selected to further characterize the electrical conductivity σ , the Seebeck coefficient S , and the power factor PF of the full polymer series **P3a–c** (Figures 3, S9). Spin-cast thin films were prepared by coprocessing *N*-DMBI with the three polymers and dopant concentrations ranging from 20 to

70 MR%. Electrical conductivity as a function of increasing dopant concentration followed a similar trend for all of the polymers (Figure 3a). Conductivity increased with increasing dopant concentration of *N*-DMBI from 20 MR% onward, after which a maximum σ_{\max} between 50 and 60 MR% appeared. Finally, conductivity decreased again at 70 MR% dopant concentrations. **P3a** exhibited lower values than its longer alkyl spacer counterparts, with a σ_{\max} for **P3a** of 0.3 S cm^{-1} at a dopant concentration of 50 MR%. Conductivities for the longer alkyl spacer counterparts **P3b** and **P3c** were twice as high compared to those of **P3a**, reaching σ_{\max} values of 0.82 and 0.83 S cm^{-1} , respectively, at dopant concentrations of 60 MR%. This represents an almost 3-fold increase in conductivity compared to similar polymers reported in the literature.³⁶

The Seebeck coefficients of the polymer-dopant blends were characterized using a custom-built setup that employed a quasi-static measurement method (Figure 3b, details are reported in the Supporting Information).⁵⁰ The Seebeck coefficients of the polymers were found to have the largest magnitude at the lowest dopant concentration, 20 MR%, with $S_{\text{P3a}} = -98.9 \mu\text{V K}^{-1}$ being the largest of the three polymers. As dopant concentration increases, the magnitude of the Seebeck coefficient decreases for all three polymers, which agrees well with the empirical relationship between thermovoltage and charge carrier concentrations seen throughout the literature.^{51,52} At dopant concentrations greater than 40 MR%, the order of Seebeck coefficients was $S_{\text{P3a}} > S_{\text{P3b}}, S_{\text{P3c}}$, while $\sigma_{\text{P3a}} < \sigma_{\text{P3b}}, \sigma_{\text{P3c}}$, indicating that the increased length of the alkyl spacer improves electrical conductivity while also slightly eroding the thermovoltage.

The power factor $\text{PF} = \sigma S^2$ was calculated for each sample and showed a trend similar to the electrical conductivity, namely that polymers **P3b** and **P3c** with longer distances between backbone and oxygen yielded higher PFs compared to **P3a**. That being said, **P3b**, the polymer with the intermediate spacer length, demonstrated the best thermoelectric performance out of the series with a $\text{PF}_{\text{P3b}} > 0.1 \mu\text{W m}^{-1} \text{ K}^{-2}$. The exact nature of the thermoelectric improvement with respect to spacer length is not known from these results alone, but it is logical to argue that an increasing side chain length allows the polymer matrix to host a larger number amount of dopant cations.⁵³ Additionally, oxygen in the side chain provides two electron lone pairs that may interact with dopant cations.

3.3. Investigation of Polymer Morphologies in Pristine and Doped States. To correlate changes in electrical performance and morphology as well as evaluate

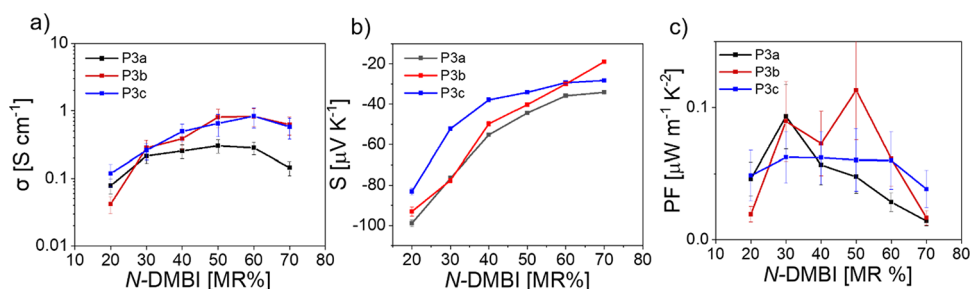


Figure 3. (a) Electrical conductivity of coprocessed thin films of **P3a–c** with respect to *N*-DMBI dopant concentration. (b) Seebeck coefficient of coprocessed thin films **P3a–c** with respect to *N*-DMBI dopant concentration. (c) Power factors of **P3a–c** versus *N*-DMBI dopant concentration calculated from conductivity and Seebeck coefficients. Error bars for electrical conductivity values arise from the experimental error of the film thickness measurement and do not represent a standard deviation.

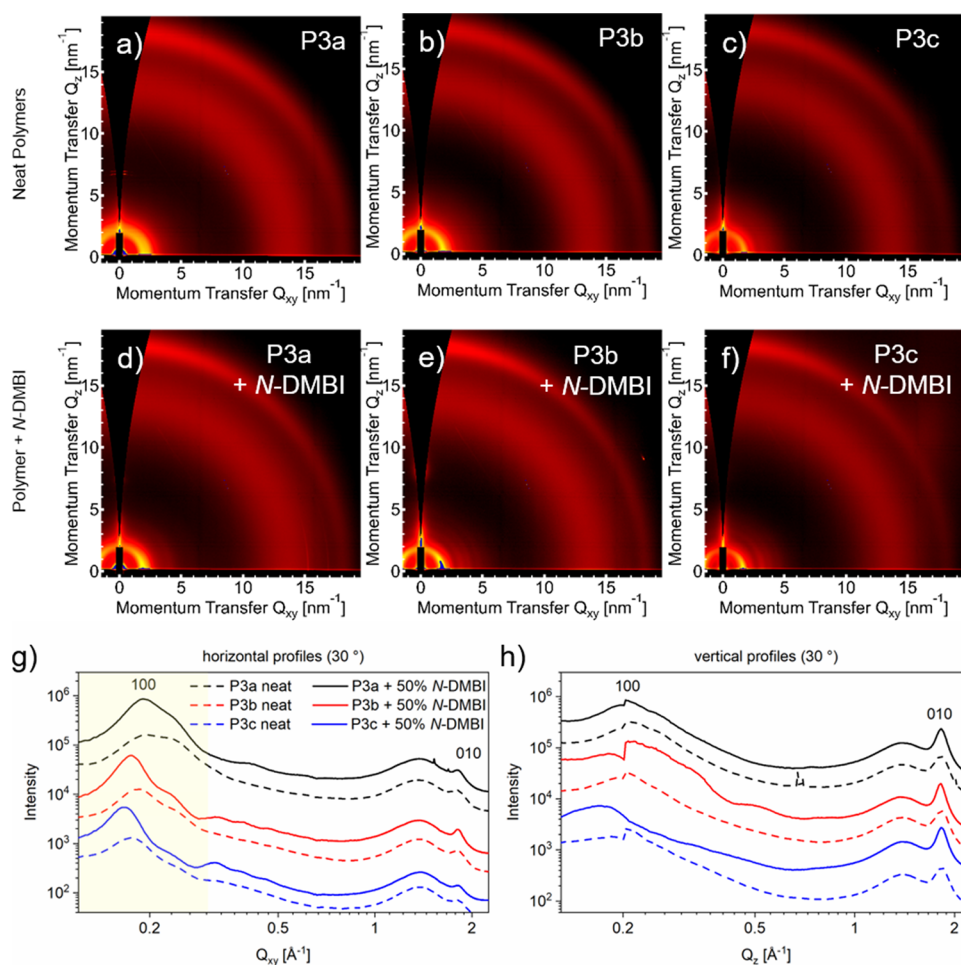


Figure 4. 2D GIWAXS images of the neat polymers **P3a**, **P3b** and **P3c** (a–c) and the respective blends with 50% *N*-DMBI (d–f) and the respective line profiles. Profiles were extracted in horizontal (g) and vertical (h) directions and are depicted in dashed lines for the neat films and solid lines for the *N*-DMBI blends. The 100 side-chain stacking peaks that change significantly during doping and side chain substitution are highlighted in the horizontal profiles. The line cuts were offset for clarity.

the microstructure of blends of the polymers with the dopant *N*-DMBI, grazing incidence wide-angle scattering (GIWAXS) experiments were conducted (Figure 4). From the observed 2D scattering patterns (Figure 4a–f), the polymers can be considered to be weakly ordered as a result of slightly curved backbones. For all polymers, side-chain stacking peaks can be observed predominantly in-plane at $\sim 0.2 \text{ \AA}^{-1}$, while a well-defined 010 π -stacking peak can be seen predominantly out-of-plane at $\sim 1.75 \text{ \AA}^{-1}$. The observations indicate a preferential “face-on” packing of chains within a morphology characterized by a high degree of mosaicity, that is, a broad distribution of the orientation of crystallites. A prominent amorphous halo is also observed 1.4 \AA^{-1} suggesting a sizable amorphous fraction. The position of the 100 peaks systematically shifts to a lower Q value going from **P3a** to **P3b** to **P3c**, which corresponds to an increasing side-chain stacking distance, consistent with the increase in the length of the alkyl side chain spacer (Figure 4g, dashed lines). This correlation matches the expected behavior, as an increase in side-chain volume consequently should lead to an increased distance of the side-chain domains. The position of the 010 peaks, in contrast, does not change between the three materials (Figure 4h, dashed lines), indicating that the π - π stacking behavior is not affected by the modification of the side chains.

Structural changes upon doping are visible both in the 2D scattering patterns and in the line profiles. When the pristine polymers are compared to the respective blend (Figure 4g, h, solid lines), a shift to smaller Q -values or a larger real space distance is observable in the 100 peaks, while the 010 signals remain unaffected. We ascribe this to a preferential accumulation of *N*-DMBI in the side-chain regions. Such an effect has been observed for polymers without OEG-substituted polymers before.

The lamellar expansion, however, is relatively small. Considering the high amount of *N*-DMBI added, we conclude that the majority of dopant is located in the amorphous domains of the polymer, which are not represented as sharp signals in the scattering patterns. If the relative shifts of the 100 peaks upon doping of the three polymers are compared, a relatively small change is observable for **P3a**, while **P3b** and **P3c** both experience a larger lamellar volume expansion. This would suggest that a higher amount of *N*-DMBI is incorporated into the crystalline domains of **P3b** and **P3c**, which is reflected in their superior conductivity (cf. Figure 4a). Interestingly, the scattering features appear to become sharper with doping, suggesting that the inclusion of the dopant leads to an increase in structural order, which is unusual. We also note there are additional peaks at low Q close to the 100 peak

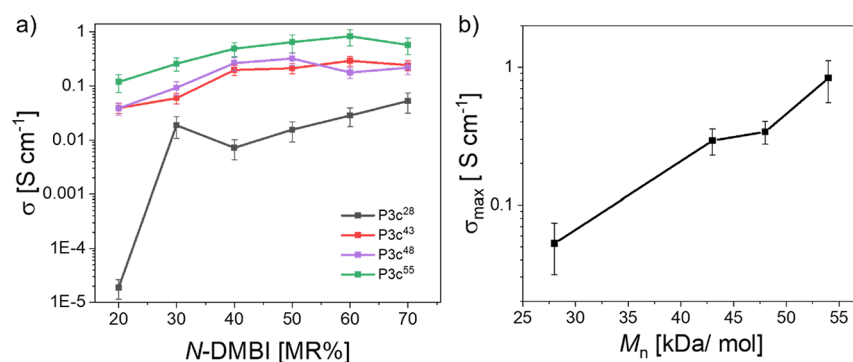


Figure 5. (a) Electrical conductivity of P3c thin films versus *N*-DMBI dopant concentration for four different M_n . (b) Electrical conductivity versus M_n at a doping concentration of *N*-DMBI = 60 MR%. Error bars for electrical conductivity values arise from the experimental error of the film thickness measurement and do not represent a standard deviation.

that are difficult to index, suggesting either the presence of a polymorph or a more complicated packing geometry.

3.4. Correlation of Molar Mass and Conductivity. As the ether side chains induce a high solubility and therefore enable the synthesis of longer chains, we further evaluate the relationship between molar mass and conductivity. Since polycondensation is governed by the Carothers equation, different M_n values are achieved by a stoichiometric imbalance of the BDF-based comonomer (Figures 5, S2). For each molecular weight obtained, conductivities were determined depending on varying doping levels of 20% < MR < 70%, showing similar trends. The sample with the lowest molar mass stood out and showed very low conductivity for low levels of doping, which increased by 3 orders of magnitude to 10⁻² S/cm.

Clearly, with P3c²⁸ reaching a σ_{max} of 0.05 S cm⁻¹ only at high *N*-DMBI concentrations of 70 MR%, a certain threshold molar mass must be reached (Figure 5a). For all larger molecular weights probed, conductivities spanned around 1 order of magnitude. Upon comparison of conductivities of the four polymers at 60 MR%, P3c⁴³ and P3c⁴⁶ exhibited both $\sigma_{\text{max}} \approx 0.35$ S cm⁻¹, while for P3c⁵⁵ a $\sigma_{\text{max}} = 0.83$ S cm⁻¹ is measured, highlighting the importance of a high solubility for the preparation of high molar mass materials (Figure 5b). To the best of our knowledge, the conductivity obtained from doped P3c⁵⁵ is the highest reported for BDF copolymers featuring nonfunctionalized isatin units, demonstrating that simple building blocks can achieve competitive performance when solubility allows long chains to form.

4. CONCLUSIONS

In summary, the work presented here introduces aliphatic side chains containing a single ether functionality for solubilizing conjugated polymers with BDF-isatin cores. The side chains are simple to make; their synthesis is scalable, and the resulting copolymers with thiophene as a comonomer exhibit excellent solubilities of up to 92 mg/mL in common organic solvents. The high solubilities allow for the preparation of a series of copolymers with different molar masses to explore molecular weight-property relationships. Here, the largest molar mass sample delivers the highest conductivity, with values of $\sigma \approx 1$ S cm⁻¹ after *n*-doping, highlighting the importance of solubility and molar mass control. Such electrical conductivities are superior compared to similar reported copolymers having unsubstituted BDF-isatin cores. GIWAXS analysis of the morphology of the copolymers reveals a high degree of

“face-on” packing, as well as a preferential location of the dopant cations in the amorphous regions, along with an increase in the structural order upon doping. The presented side chains can easily be used for a variety of other copolymers where branching point variation is of interest and where solubility limits molar mass.

ASSOCIATED CONTENT

Supporting Information

The Supporting Information is available free of charge at <https://pubs.acs.org/doi/10.1021/acsapm.3c02137>.

All synthetic procedures, characterization data (NMR spectroscopy and mass spectrometry), and descriptions of experimental methods; additional figures, schemes, and tables; NMR spectra, SEC curves, UV-vis spectra, cyclic voltammograms, conductivity data, Seebeck coefficients, and power factors (DOCX)

AUTHOR INFORMATION

Corresponding Authors

Mario Caironi – Center for Nano Science and Technology, 20134 Milano, Italy; orcid.org/0000-0002-0442-4439; Email: mario.caironi@iit.it

Michael Sommer – Institut für Chemie, Technische Universität Chemnitz, 09111 Chemnitz, Germany; Forschungszentrum MAIN, TU Chemnitz, 09126 Chemnitz, Germany; orcid.org/0000-0002-2377-5998; Email: michael.sommer@chemie.tu-chemnitz.de

Authors

Diego R. Hinojosa – Institut für Chemie, Technische Universität Chemnitz, 09111 Chemnitz, Germany; Forschungszentrum MAIN, TU Chemnitz, 09126 Chemnitz, Germany; orcid.org/0000-0002-4849-2062

Nathan J. Pataki – Center for Nano Science and Technology, 20134 Milano, Italy; Department of Physics, Politecnico di Milano, 20133 Milano, Italy; orcid.org/0000-0002-3691-5427

Pietro Rossi – Center for Nano Science and Technology, 20134 Milano, Italy; Department of Physics, Politecnico di Milano, 20133 Milano, Italy

Andreas Erhardt – Department of Materials Science and Engineering, Monash University, Clayton, Victoria 3800, Australia

Shubhradip Guchait – Institute Charles Sadron, Université de Strasbourg, Strasbourg F-67000, France

Francesca Pallini – Department of Materials Science, Università di Milano-Bicocca, 20125 Milan, Italy
Christopher McNeill – Department of Materials Science and Engineering, Monash University, Clayton, Victoria 3800, Australia; orcid.org/0000-0001-5221-878X
Christian Müller – Department of Chemistry and Chemical Engineering, Chalmers University of Technology, Göteborg 412 96, Sweden; orcid.org/0000-0001-7859-7909

Complete contact information is available at:
<https://pubs.acs.org/10.1021/acsapm.3c02137>

Author Contributions

The manuscript was written through contributions of all authors. All authors have given approval to the final version of the manuscript.

Funding

This project has received funding from the European Union's Horizon 2020 research and innovation program under the Marie Skłodowska-Curie grant agreement No 955837 – HORATES.

Notes

The authors declare no competing financial interest.

ACKNOWLEDGMENTS

The authors thank Dr. Anders Mårtensson for SEC measurements, Dr. Rukiya Matsidik for MALDI-TOF measurements, and Prof. Luca Beverina for support in the synthesis of the N-DMBI dopant. D.R.H. thanks Dominik Stegerer for support in CV measurements, Raphael Hertel for support in UV-vis measurements, and Monika Shamsabadi and Joost Kimpel for fruitful discussions and correcting the manuscript. This work was performed in part at the SAXS/WAXS beamline at the Australian Synchrotron, part of ANSTO.⁵⁴

REFERENCES

- (1) Rasmussen, S. C. Conjugated and Conducting Organic Polymers: The First 150 Years. *ChemPlusChem* **2020**, *85* (7), 1412–1429.
- (2) Bao, Z.; Chan, W. K.; Yu, L. Exploration of the Stille Coupling Reaction for the Synthesis of Functional Polymers. *J. Am. Chem. Soc.* **1995**, *117* (50), 12426–12435.
- (3) Mei, J.; Bao, Z. Side Chain Engineering in Solution-Processable Conjugated Polymers. *Chem. Mater.* **2014**, *26* (1), 604–615.
- (4) Jiang, H.; Taranekekar, P.; Reynolds, J. R.; Schanze, K. S. Conjugated Polyelectrolytes: Synthesis, Photophysics, and Applications. *Angew. Chem., Int. Ed.* **2009**, *48* (24), 4300–4316.
- (5) Ma, W.; Iyer, P. K.; Gong, X.; Liu, B.; Moses, D.; Bazan, G. C.; Heeger, A. J. Water/Methanol-Soluble Conjugated Copolymer as an Electron-Transport Layer in Polymer Light-Emitting Diodes. *Adv. Mater.* **2005**, *17* (3), 274–277.
- (6) Liu, F.; Zhao, X.; Zhang, X.; Zhang, X.; Peng, J.; Yang, H.; Deng, K.; Ma, L.; Chang, C.; Wei, H. Fabrication of Thera-nostic Amphiphilic Conjugated Bottlebrush Copolymers with Alternating Heterografts for Cell Imaging and Anticancer Drug Delivery. *Polym. Chem.* **2018**, *9* (39), 4866–4874.
- (7) Png, R.-Q.; Chia, P.-J.; Tang, J.-C.; Liu, B.; Sivaramakrishnan, S.; Zhou, M.; Khong, S.-H.; Chan, H. S.; Burroughes, J. H.; Chua, L.-L.; Friend, R. H.; Ho, P. K. High-Performance Polymer Semiconducting Heterostructure Devices by Nitrene-Mediated Photocrosslinking of Alkyl Side Chains. *Nat. Mater.* **2010**, *9* (2), 152–158.
- (8) Miyanishi, S.; Tajima, K.; Hashimoto, K. Morphological Stabilization of Polymer Photovoltaic Cells by Using Cross-Linkable Poly(3-(5-Hexenyl)Thiophene). *Macromolecules* **2009**, *42* (5), 1610–1618.
- (9) Jakob, S.; Moreno, A.; Zhang, X.; Bertschi, L.; Smith, P.; Schlüter, A. D.; Sakamoto, J. Synthesis of Polyphenylenes from a Soluble Precursor: The “Shaving” Approach. *Macromolecules* **2010**, *43* (19), 7916–7918.
- (10) Bundgaard, E.; Hagemann, O.; Bjerring, M.; Nielsen, N. Chr.; Andreasen, J. W.; Andreasen, B.; Krebs, F. C. Removal of Solubilizing Side Chains at Low Temperature: A New Route to Native Poly(Thiophene). *Macromolecules* **2012**, *45* (8), 3644–3646.
- (11) Shi, C.; Yao, Y.; Yang, Pei, Q. Regioregular Copolymers of 3-Alkoxythiophene and Their Photovoltaic Application. *J. Am. Chem. Soc.* **2006**, *128* (27), 8980–8986.
- (12) Ruiz, J. P.; Nayak, K.; Marynick, D. S.; Reynolds, J. R. Soluble Ethylmercapto-Substituted Polythiophenes. *Macromolecules* **1989**, *22* (3), 1231–1238.
- (13) Zhang, Q. T.; Tour, J. M. Alternating Donor/Acceptor Repeat Units in Polythiophenes. Intramolecular Charge Transfer for Reducing Band Gaps in Fully Substituted Conjugated Polymers. *J. Am. Chem. Soc.* **1998**, *120* (22), 5355–5362.
- (14) Nielsen, C. B.; Sohn, E.-H.; Cho, D.-J.; Schroeder, B. C.; Smith, J.; Lee, M.; Anthopoulos, T. D.; Song, K.; McCulloch, I. Improved Field-Effect Transistor Performance of a Benzotrithiophene Polymer through Ketall Cleavage in the Solid State. *ACS Appl. Mater. Interfaces* **2013**, *5* (5), 1806–1810.
- (15) Chen, H.-Y.; Hou, J.; Zhang, S.; Liang, Y.; Yang, G.; Yang, Y.; Yu, L.; Wu, Y.; Li, G. Polymer Solar Cells with Enhanced Open-Circuit Voltage and Efficiency. *Nat. Photonics* **2009**, *3* (11), 649–653.
- (16) Banno, M.; Yamaguchi, T.; Nagai, K.; Kaiser, C.; Hecht, S.; Yashima, E. Optically Active, Amphiphilic Poly(Meta-Phenylene Ethynylene)s: Synthesis, Hydrogen-Bonding Enforced Helix Stability, and Direct AFM Observation of Their Helical Structures. *J. Am. Chem. Soc.* **2012**, *134* (20), 8718–8728.
- (17) Li, H.; Sundararaman, A.; Venkatasubbiah, K.; Jäkle, F. Organoborane Acceptor-Substituted Polythiophene via Side-Group Borylation. *J. Am. Chem. Soc.* **2007**, *129* (18), 5792–5793.
- (18) Kline, R. J.; DeLongchamp, D. M.; Fischer, D. A.; Lin, E. K.; Richter, L. J.; Chabinc, M. L.; Toney, M. F.; Heeney, M.; McCulloch, I. Critical Role of Side-Chain Attachment Density on the Order and Device Performance of Polythiophenes. *Macromolecules* **2007**, *40* (22), 7960–7965.
- (19) Wu, Z.; Petzold, A.; Henze, T.; Thurn-Albrecht, T.; Lohwasser, R. H.; Sommer, M.; Thelakkat, M. Temperature and Molecular Weight Dependent Hierarchical Equilibrium Structures in Semiconducting Poly(3-Hexylthiophene). *Macromolecules* **2010**, *43* (10), 4646–4653.
- (20) Sugiyama, F.; Kleinschmidt, A. T.; Kayser, L. V.; Rodriguez, D.; Finn, M.; Alkhadra, M. A.; Wan, J. M.-H.; Ramirez, J.; Chiang, A. S.-C.; Root, S. E.; Savagatrup, S.; Lipomi, D. J. Effects of Flexibility and Branching of Side Chains on the Mechanical Properties of Low-Bandgap Conjugated Polymers. *Polym. Chem.* **2018**, *9* (33), 4354–4363.
- (21) Kanimozhi, C.; Yaacobi-Gross, N.; Burnett, E. K.; Briseno, A. L.; Anthopoulos, T. D.; Salzner, U.; Patil, S. Use of Side-Chain for Rational Design of N-Type Diketopyrrolopyrrole-Based Conjugated Polymers: What Did We Find Out? *Phys. Chem. Chem. Phys.* **2014**, *16* (32), 17253–17265.
- (22) Wang, S.; Shaw, J.; Han, Y.; Fei, Z.; Glöcklhofer, F.; Heeney, M. Multibranch Aliphatic Side Chains for π -Conjugated Polymers with a High Density of ‘Unshielded’ Aromatics. *Chem. Commun.* **2020**, *56* (81), 12138–12141.
- (23) Nielsen, C. B.; Turbiez, M.; McCulloch, I. Recent Advances in the Development of Semiconducting DPP-Containing Polymers for Transistor Applications. *Adv. Mater.* **2013**, *25* (13), 1859–1880.
- (24) Sommer, M. Conjugated Polymers Based on Naphthalene Diimide for Organic Electronics. *J. Mater. Chem. C* **2014**, *2* (17), 3088–3098.
- (25) Fu, B.; Baltazar, J.; Sankar, A. R.; Chu, P.-H.; Zhang, S.; Collard, D. M.; Reichmanis, E. Enhancing Field-Effect Mobility of Conjugated Polymers through Rational Design of Branched Side Chains. *Adv. Funct. Mater.* **2014**, *24* (24), 3734–3744.

- (26) Lei, T.; Dou, J.-H.; Pei, J. Influence of Alkyl Chain Branching Positions on the Hole Mobilities of Polymer Thin-Film Transistors. *Adv. Mater.* **2012**, *24* (48), 6457–6461.
- (27) Yu, Z.-D.; Lu, Y.; Wang, Z.-Y.; Un, H.-I.; Zelewski, S. J.; Cui, Y.; You, H.-Y.; Liu, Y.; Xie, K.-F.; Yao, Z.-F.; He, Y.-C.; Wang, J.-Y.; Hu, W.-B.; Sirringhaus, H.; Pei, J. High N-Type and P-Type Conductivities and Power Factors Achieved in a Single Conjugated Polymer. *Sci. Adv.* **2023**, *9* (8), No. eadf3495, DOI: 10.1126/sciadv.adf3495. <https://www.science.org/doi/10.1126/sciadv.adf3495>
- (28) Shivhare, R.; Erdmann, T.; Hörmann, U.; Collado-Fregoso, E.; Zeiske, S.; Benduhn, J.; Ullbrich, S.; Hübnner, R.; Hambach, M.; Kiriy, A.; Voit, B.; Neher, D.; Vandewal, K.; Mannsfeld, S. C. Alkyl Branching Position in Diketopyrrolopyrrole Polymers: Interplay between Fibrillar Morphology and Crystallinity and Their Effect on Photogeneration and Recombination in Bulk-Heterojunction Solar Cells. *Chem. Mater.* **2018**, *30* (19), 6801–6809.
- (29) O'Lenick, A. J. Guerbet Chemistry. *J. Surfactants Deterg.* **2001**, *4* (3), 311–315.
- (30) Chan, W. K.; Chen, Y.; Peng, Z.; Yu, L. Rational Designs of Multifunctional Polymers. *J. Am. Chem. Soc.* **1993**, *115* (25), 11735–11743.
- (31) Chen, Z.; Zheng, Y.; Yan, H.; Facchetti, A. Naphthalenedi-carboximide- vs Perylenedicarboximide-Based Copolymers. Synthesis and Semiconducting Properties in Bottom-Gate N-Channel Organic Transistors. *J. Am. Chem. Soc.* **2009**, *131* (1), 8–9.
- (32) Ehsan, M.; Du, Y.; Scull, N. J.; Tikhonova, E.; Tarrasch, J.; Mortensen, J. S.; Loland, C. J.; Skiniotis, G.; Guan, L.; Byrne, B.; Kobilka, B. K.; Chae, P. S. Highly Branched Pentasaccharide-Bearing Amphiphiles for Membrane Protein Studies. *J. Am. Chem. Soc.* **2016**, *138* (11), 3789–3796.
- (33) Zheng, Y.-Q.; Yao, Z.-F.; Dou, J.-H.; Wang, Y.; Ma, W.; Zou, L.; Nikzad, S.; Li, Q.-Y.; Sun, Z.-H.; Yu, Z.-A.; Zhang, W.-B.; Wang, J.-Y.; Pei, J. Influence of Solution-State Aggregation on Conjugated Polymer Crystallization in Thin Films and Microwire Crystals. *Giant* **2021**, *7*, No. 100064.
- (34) Tang, H.; Liang, Y.; Liu, C.; Hu, Z.; Deng, Y.; Guo, H.; Yu, Z.; Song, A.; Zhao, H.; Zhao, D.; Zhang, Y.; Guo, X.; Pei, J.; Ma, Y.; Cao, Y.; Huang, F. A solution-processed n-type conducting polymer with ultrahigh conductivity. *Nature* **2022**, *611*, 271–277.
- (35) Ke, Z.; Abtahi, A.; Hwang, J.; Chen, K.; Chaudhary, J.; Song, I.; Perera, K.; You, L.; Baustert, K. N.; Graham, K. R.; Mei, J. Highly Conductive and Solution-Processable n-Doped Transparent Organic Conductor. *J. Am. Chem. Soc.* **2023**, *145* (6), 3706–3715.
- (36) Shi, K.; Zhang, F.; Di, C.-A.; Yan, T.-W.; Zou, Y.; Zhou, X.; Zhu, D.; Wang, J.-Y.; Pei, J. Toward High Performance n-Type Thermoelectric Materials by Rational Modification of BDPPV Backbones. *J. Am. Chem. Soc.* **2015**, *137* (22), 6979–6982.
- (37) Lei, T.; Xia, X.; Wang, J.-Y.; Liu, C.-J.; Pei, J. Conformation Locked[†] Strong Electron-Deficient Poly(*p*-Phenylene Vinylene) Derivatives for Ambient-Stable N-Type Field-Effect Transistors: Synthesis, Properties, and Effects of Fluorine Substitution Position. *J. Am. Chem. Soc.* **2014**, *136* (5), 2135–2141.
- (38) Dai, Y.-Z.; Ai, N.; Lu, Y.; Zheng, Y.-Q.; Dou, J.-H.; Shi, K.; Lei, T.; Wang, J.-Y.; Pei, J. Embedding Electron-Deficient Nitrogen Atoms in Polymer Backbone towards High Performance N-Type Polymer Field-Effect Transistors. *Chemical Science* **2016**, *7* (9), 5753–5757.
- (39) Zhang, W.; Mao, Z.; Chen, Z.; Huang, J.; Wei, C.; Gao, D.; Lin, Z.; Li, H.; Wang, L.; Yu, G. Ambipolar Tetrafluorodiphenylethene-Based Donor–Acceptor Copolymers: Synthesis, Properties, Backbone Conformation and Fluorine-Induced Conformational Locks. *Polym. Chem.* **2017**, *8* (5), 879–889.
- (40) Qiao, Y.; Guo, Y.; Yu, C.; Zhang, F.; Xu, W.; Liu, Y.; Zhu, D. Diketopyrrolopyrrole-Containing Quinoidal Small Molecules for High-Performance, Air-Stable, and Solution-Processable n-Channel Organic Field-Effect Transistors. *J. Am. Chem. Soc.* **2012**, *134* (9), 4084–4087.
- (41) Lei, T.; Dou, J.-H.; Cao, X.-Y.; Wang, J.-Y.; Pei, J. Electron-Deficient Poly(*p*-Phenylene Vinylene) Provides Electron Mobility over 1 Cm² V^{−1} s^{−1} under Ambient Conditions. *J. Am. Chem. Soc.* **2013**, *135* (33), 12168–12171.
- (42) Dou, J.-H.; Zheng, Y.-Q.; Lei, T.; Zhang, S.-D.; Wang, Z.; Zhang, W.-B.; Wang, J.-Y.; Pei, J. Systematic Investigation of Side-Chain Branching Position Effect on Electron Carrier Mobility in Conjugated Polymers. *Adv. Funct. Mater.* **2014**, *24* (40), 6270–6278.
- (43) Wang, X.; Liu, Y.; Wang, Z.; Lu, Y.; Yao, Z.; Ding, Y.; Yu, Z.; Wang, J.; Pei, J. Revealing the Effect of Oligo(Ethylene Glycol) Side Chains on N-doping Process in Fbdppv-based Polymers. *J. Polym. Sci.* **2022**, *60* (3), 538–547.
- (44) He, Y.; Guo, C.; Sun, B.; Quinn, J.; Li, Y. Branched Alkyl Ester Side Chains Rendering Large Polycyclic (3E,7E)-3,7-Bis(2-Oxindolin-3-Ylidene)Benzo[1,2-b:4,5-b']Difuran-2,6(3h,7h)-Dione (IBDF) Based Donor–Acceptor Polymers Solution-Processability for Organic Thin Film Transistors. *Polym. Chem.* **2015**, *6* (37), 6689–6697.
- (45) Bardagot, O.; Kubik, P.; Marszalek, T.; Veyre, P.; Medjahed, A. A.; Sandroni, M.; Grévin, B.; Pouget, S.; Nunes Domschke, T.; Carella, A.; Gambarelli, S.; Pisula, W.; Demadrille, R. Impact of Morphology on Charge Carrier Transport and Thermoelectric Properties of N-Type FBDOPV-based Polymers. *Adv. Funct. Mater.* **2020**, *30* (21), No. 2000449.
- (46) Venkateshvaran, D.; Nikolka, M.; Sadhanala, A.; Lemaire, V.; Zelazny, M.; Kepa, M.; Hurhangee, M.; Kronemeijer, A. J.; Pecunia, V.; Nasrallah, I.; Romanov, I.; Broch, K.; McCulloch, I.; Emin, D.; Olivier, Y.; Cornil, J.; Beljonne, D.; Sirringhaus, H. Approaching Disorder-Free Transport in High-Mobility Conjugated Polymers. *Nature* **2014**, *515* (7527), 384–388.
- (47) Cao, Z.; Ma, G.; Leng, M.; Zhang, S.; Chen, J.; Do, C.; Hong, K.; Fang, L.; Gu, X. Variable-Temperature Scattering and Spectroscopy Characterizations for Temperature-Dependent Solution Assembly of PFFBT4T-Based Conjugated Polymers. *ACS Applied Polymer Materials* **2022**, *4* (5), 3023–3033.
- (48) Shin, Y.; Massetti, M.; Komber, H.; Biskup, T.; Nava, D.; Lanzani, G.; Caironi, M.; Sommer, M. Improving Miscibility of a Naphthalene Diimide-Bithiophene Copolymer with N-Type Dopants through the Incorporation of “Kinked” Monomers. *Advanced Electronic Materials* **2018**, *4* (10), No. 1700581.
- (49) Nava, D.; Shin, Y.; Massetti, M.; Jiao, X.; Biskup, T.; Jagadeesh, M. S.; Calloni, A.; Duò, L.; Lanzani, G.; McNeill, C. R.; Sommer, M.; Caironi, M. Drastic Improvement of Air Stability in an N-Type Doped Naphthalene-Diimide Polymer by Thionation. *ACS Applied Energy Materials* **2018**, *1* (9), 4626–4634.
- (50) Beretta, D.; Bruno, P.; Lanzani, G.; Caironi, M. Reliable Measurement of the Seebeck Coefficient of Organic and Inorganic Materials between 260 and 460 K. *Rev. Sci. Instrum.* **2015**, *86* (7), No. 075104.
- (51) Gregory, S. A.; Hanus, R.; Atassi, A.; Rinehart, J. M.; Wooding, J. P.; Menon, A. K.; Losego, M. D.; Snyder, G. J.; Yee, S. K. Quantifying Charge Carrier Localization in Chemically Doped Semiconducting Polymers. *Nat. Mater.* **2021**, *20* (10), 1414–1421.
- (52) Russ, B.; Gludell, A.; Urban, J. J.; Chabinyk, M. L.; Segalman, R. A. Organic Thermoelectric Materials for Energy Harvesting and Temperature Control. *Nat. Rev. Mater.* **2016**, *1* (10), 16050 DOI: 10.1038/natrevmats.2016.50.
- (53) Li, Q.; Yao, Z.; Wu, H.; Luo, L.; Ding, Y.; Yang, C.; Wang, X.; Shen, Z.; Wang, J.; Pei, J. Regulation of High Miscibility for Efficient Charge-transport in N-doped Conjugated Polymers. *Angew. Chem., Int. Ed.* **2022**, *61* (14), No. e202200221.
- (54) Kirby, N. M.; Mudie, S. T.; Hawley, A. M.; Cookson, D. J.; Mertens, H. D.; Cowieson, N.; Samardzic-Boban, V. A Low-Background-Intensity Focusing Small-Angle X-Ray Scattering Undulator Beamline. *J. Appl. Crystallogr.* **2013**, *46* (6), 1670–1680.